Can. J. Remote Sensing, Vol. 34, No. 3, pp. 174–191, 2008

Refining a hyperspectral and multiangle measurement concept for vegetation structure assessment

A. Simic and J.M. Chen

Abstract. The concept of combining multiangle and hyperspectral remote sensing has been developed and utilized in the compact high-resolution imaging spectrometer (CHRIS) satellite observation system onboard the project for on-board autonomy (PROBA) platform developed by the European Space Agency (ESA). Recent studies show that this technology is useful for extracting crop and soil information, and it is very promising for deriving forest structural and biochemical parameters. However, hyperspectral measurements at multiple angles appear to have much redundancy. Therefore, we attempt to refine this measurement concept by testing a new system that acquires hyperspectral signals only in the nadir direction but measures in two additional directions in two spectral bands, namely red and near-infrared (NIR). According to our recent research, we propose that the best two view angles are (*i*) the hotspot, where the Sun and view directions coincide; and (*ii*) the darkspot, where the sensor sees the maximum amount of vegetation structural shadows. Through model experiments, we demonstrate that the combination of the hotspot and darkspot reflectances has the strongest signals about the vegetation structure quantified using the foliage clumping index. The 5-Scale model is used in this study to simulate CHRIS data. Very good agreements are shown between modelled and CHRIS-measured spectra at the nadir and off-nadir view angles, except for the largest view angle (+55°), at which the atmospheric correction is uncertain. Furthermore, we successfully demonstrate that the off-nadir hyperspectral simulations could be brought in very close agreement with the CHRIS data once multispectral measurements at the same off-nadir angles are available. In other words, all hyperspectral bands can be closely reconstructed based on the nadir hyperspectral reflectance and off-nadir multispectral reflectance in the red and NIR bands. This is shown for black spruce and aspen forests using the CHRIS data acquired over the Sudbury region in Canada. The results suggest that the multiangle hyperspectral data exhibit much redundancy, and that the multispectral measurements at off-nadir angles in addition to the nadir hyperspectral data would be sufficient to reconstruct hyperspectral signatures at off-nadir angles. This proposed concept could be regarded as a refinement of the existing sensor. Remote sensing data acquired using this new measurement concept would provide the opportunity to analyze simultaneously vegetation structural and biochemical information.

Résumé. Le concept de la combinaison de la télédétection multiangulaire et hyperspectrale a été développé et utilisé dans un système satellitaire d'observation existant, le système CHRIS (« compact high-resolution imaging spectrometer »), à bord de la plateforme PROBA (« project for on-board autonomy ») développée par l'Agence spatiale européenne (ESA). Des études récentes montrent que cette technologie est utile pour extraire l'information sur les cultures et le sol, et qu'elle est très prometteuse pour dériver les paramètres structurels et biochimiques de la forêt. Cependant, les mesures hyperspectrales à angles multiples semblent présenter beaucoup de redondance. Ainsi, nous tentons de raffiner ce concept de mesure en en testant un nouveau : un système qui acquiert des signaux hyperspectraux uniquement dans la direction au nadir mais qui mesure dans deux autres directions en deux bandes spectrales, le rouge et le PIR. En fonction de nos recherches récentes, nous proposons que les deux meilleurs angles de visée sont : (*i*) le point anti-spéculaire, où le soleil et les directions de visée coïncident et (*ii*) le point sombre, où le capteur voit le nombre maximal d'ombres des structures végétales. En expérimentant avec des modèles, nous démontrons que la combinaison des réflectances du point anti-spéculaire et du point sombre affiche les signaux les plus forts quant à la structure de la végétation quantifiée en utilisant un indice d'agrégation du feuillage. Le modèle 5-Scale est utilisé dans cette étude pour simuler les données de CHRIS. De très bonnes corrélations sont démontrées entre les spectres modélisés et ceux mesurés par CHRIS aux angles de visée au nadir et en oblique, excepté pour le plus grand angle de visée (+55°) pour lequel la correction atmosphérique est incertaine. De plus, nous démontrons avec succès que les simulations hyperspectrales en oblique pourraient être amenées à des niveaux de corrélation très proches avec les données de CHRIS, une fois que les mesures multispectrales aux mêmes angles en oblique sont disponibles. En d'autres mots, toutes les bandes hyperspectrales peuvent être reconstruites assez fidèlement basé sur la réflectance hyperspectrale au nadir et la réflectance multispectrale en oblique dans les bandes du rouge et du PIR. Ceci est

Received 17 January 2008. Accepted 7 April 2008. Published on the *Canadian Journal of Remote Sensing* Web site at http://pubs.nrc-cnrc.gc.ca/cjrs on 21 August 2008.

A. Simic[1] and J.M. Chen. Department of Geography, University of Toronto, 100 St. George Street, Toronto, ON M5S 3G3, Canada.

[1]Corresponding author (e-mail: simica@geog.utoronto.ca).

démontré pour les forêts d'épinette noire et de tremble en utilisant les données de CHRIS acquises au-dessus de la région de Sudbury, au Canada. Les résultats laissent supposer que les données hyperspectrales multiangulaires affichent beaucoup de redondance et que les mesures multispectrales aux angles en oblique en plus des données hyperspectrales au nadir seraient suffisantes pour reconstruire les signatures hyperspectrales aux angles en oblique. Le concept proposé pourrait être considéré comme un raffinement du capteur existant. Les données de télédétection acquises à l'aide de ce nouveau concept de mesure fournirait l'opportunité d'analyser simultanément l'information structurelle et biochimique.
[Traduit par la Rédaction]

Introduction

This study seeks to explore the concept of simultaneous utilization of multiangle and hyperspectral measurements for vegetation information retrieval. It is well known that hyperspectral remote sensing systems provide unique means for retrieving the biophysical and biochemical parameters of the land surface (Treitz and Howarth 1999; Smith et al., 2003; Townsend et al., 2003). It has also been shown that the angular variations of surface reflectance contain information on the structure of vegetated surfaces (Deering et al., 1999; Sandmaier and Deering, 1999; Zhang et al., 2002; Chen et al., 2003; Gao et al., 2003; Cierniewsky et al., 2004; Rautiainen et al., 2004; Bach et al., 2005; Widlowski et al., 2004). The concept of combining multiangle and hyperspectral remote sensing has been successfully utilized in an existing satellite observation system named the compact high-resolution imaging spectrometer (CHRIS) onboard the project for on-board autonomy (PROBA), a highly manoeuvrable small satellite of the European Space Agency (ESA). In addition to fine spectral resolution, the ability to provide multiangular views of the same scene is a very distinct feature of this sensor. This feature is particularly useful in providing vegetation information, including plant biophysical (leaf area index) and biochemical (chlorophyll, water, and nitrogen content) parameters (Begiebing et al., 2005). The ESA is developing a new multiangle hyperspectral sensor SPECTRA with a possible launch date in 2008, and the Canadian Space Agency also has a potential to develop a hyperspectral sensor HERO in a similar time frame.

The CHRIS instrument has a spectral range from 400 to 1050 nm, with spectral resolutions <11 nm. The instrument provides five sets of images of a target area in a single overpass with a ground sampling resolution of 17 or 34 m. It can operate in five modes. Mode 1 covers the full path swath of 13.4 km, with 62 bands acquired at a 34 m ground sampling distance at nadir. Mode 2 has 18 water bands acquired at 17 m. Modes 3 and 5 incorporate 18 and 37 land channels, respectively, and they are acquired at 17 m. Mode 5 has half the swath width, and mode 3 covers the full swath. Mode 4 is called the chlorophyll band set; it covers the full swath and has 18 bands collected at 17 m. The platform acquires images at an altitude of about 550–670 km when the zenith angle of the platform with respect to the fly-by position is equal to a set of fly-by zenith angles (FZAs): 0°, ±36°, and ±55° (Barnsley et al., 2004; Cutter, 2004; Guanter et al., 2005a). CHRIS provides unique and complimentary measurements of the Earth's surface in the spectral, spatial, and angular remote sensing domains. Recent analyses of CHRIS data show that this technology is useful in extracting crop and soil information (Begiebing et al., 2005; Bach et al., 2005). It is also very promising for retrieving vegetation structural information, such as leaf area index (LAI) in particular (Lewis et al., 2001; Vuolo et al., 2005; D'Urso et al., 2004). Reflectance models are often inverted to retrieve LAI values for different agricultural crops. CHRIS multiangle data over one overpass also improve the accuracies of forest species recognition and stand density estimation when compared with the case with only nadir view data (Dyk et al., 2005; Goodenough et al., 2005; Schlerf and Hill, 2005).

Although is it expected that such data will greatly improve the derivation of biophysical and biochemical parameters of the surface, there are a number of challenges that have to be overcome before they are used for information retrieval. Numerous studies emphasize high redundancy among hyperspectral bands within a single view. Due to large data dimensions, there are numerous methods for hyperspectral data compression by exploiting the redundancy (Kumar and Makkapati, 2005; Motta, et al., 2006; Costa and Fiori, 2001). A goal of many studies is to identify those bands which contain needed information with minimal redundancy for specific applications (Bajwa et al., 2004; Guo et al., 2005). Particular attention has been given to the redundancy reduction in the case of land cover recognition (Dyk et al., 2005; Goodenough et al., 2005). Vuolo et al. (2005) found that only a limited number of CHRIS bands, in particular, were compulsory for biophysical variable estimation and that noise was added with any additional bands. In any case, there is a tendency to recognize the useful wavelength and to reduce the redundant information. Hyperspectral measurements in multiple look directions also appear to have much redundancy, and there is also a question of what are the best angles to look at the surface for general applications.

Based on the existing CHRIS data and results, we propose to refine the present multiangle and hyperspectral measurement concept by testing a new concept: a system that acquires hyperspectral signals only in the nadir direction but measures in two additional directions in two spectral bands, namely red and near-infrared (NIR). According to the recent study of Chen et al. (2005), it was found that the two best view directions for assessing the canopy structure are hotspot and darkspot. The hotspot is a geometric–optical effect denoting the backscatter peak in directional reflectance hemisphere where illumination and view

directions coincide, resulting in the absence of visible shadows. The darkspot reflectance, on the other hand, contains the maximum visible shadows observed in the forward-scattering direction, where the reflectance is minimum. The combination of the hotspot and darkspot views has the strongest signals about the vegetation structure. Assuming that it is technologically feasible to synchronize the camera look directions in space with the Sun angle to acquire images near the hotspot and darkspot, the purpose of this study is to test this refined concept of measurements using an existing CHRIS dataset.

The overall goal of our research on this new measurement concept is to demonstrate its capability for simultaneous retrieval of both vegetation structural and biochemical parameters, including LAI, clumping index, and leaf chlorophyll content. To achieve this goal, we conducted research in the following three stages: (*i*) to demonstrate that multispectral measurements at two off-nadir angles, in addition to nadir hyperspectral data, are sufficient for retrieving canopy structural parameters, and that the best two off-nadir angles are the hotspot and the darkspot; (*ii*) to demonstrate that, given nadir hyperspectral and off-nadir multispectral measurements, the hyperspectral signals at off-nadir angles can be well simulated using a model, proving the argument that no substantial information is gained from hyperspectral measurements of vegetated areas at more than one angle; and (*iii*) to demonstrate improvement in chlorophyll retrieval at canopy level based on the improved biophysical parameters once two optimal off-nadir angles data are added to nadir hyperspectral data.

Results from the first two stages of this research are presented in this paper, and those from the third stage will be shown in a separate publication. The hyperspectral geometrical optical model 5-Scale (Chen and Leblanc, 2001) is the main tool for this investigation. Specifically, we perform the following tasks:

(1) We show the ability and the error ranges of 5-Scale in simulating hyperspectral signals at CHRIS view angles and the ability of the model to simulate hyperspectral signals at various angles once the model is calibrated to the nadir hyperspectral data.

(2) We show that, due to the data redundancy, the CHRIS data at off-nadir views could be reconstructed for forested areas (the most complex case) by the multispectral red and NIR measurements in addition to a given hyperspectral nadir view.

(3) We develop a method for hotspot determination. As it is not possible to measure exactly at the hotspot for all pixels in an image due to orbital constraints, we need a methodology to extrapolate an angular point near the hotspot to the actual hotspot within CHRIS data. We also need to assess the error of extrapolation in relation to the angular distance of the measurement from the hotspot.

(4) We demonstrate, through model simulations and initial validation against ground data, that the best two angles of view, in addition to nadir, are hotspot and darkspot. We demonstrate that multispectral measurements at off-nadir angles, in addition to nadir hyperspectral data, provide optimal retrieval accuracy of clumping index.

In addition to its relevance for future satellite sensor designs, the outcome of this research would immediately help utilize CHRIS data for vegetation structural information retrieval. The foliage clumping index retrieval investigated in this research is a parameter useful for vegetation net primary productivity modelling, which is a critical component of the terrestrial carbon cycle. Leaves in plant canopies, especially in forests and shrubs, are generally highly clumped, meaning that leaves are more overlapped vertically than the random case because of canopy structures such as crowns, whirls, branches, and shoots. This clumping decreases sunlit leaves and increases shaded leaves at all Sun angles. It also affects the radiation reaching the background surface under the canopy. The foliage clumping index, therefore, is of equal importance to LAI for carbon–water cycle modelling. Chen et al. (2005) developed the normalized difference between hotspot and darkspot (NDHD), an angular index to characterize the anisotropic behaviour of foliage components. It incorporates the reflectance at the hotspot and darkspot. This index was successfully related to ground-based measurements of the clumping index of conifer forests, deciduous forests, and grassland (Chen et al., 2005). The relationship was found to be significant for the red and NIR wavelengths when the crown envelope coverage of the ground in a forest exceeds 25% (Chen et al., 2005).

Modelling

The 5-Scale model is a geometric–optical radiative-transfer model with emphasis on the structural composition of forest canopies at different scales, including tree groups, tree crown shapes, branches, shoots, and leaf cells. The main purpose of the model is to compute the reflectance of a vegetated surface. The model can be applied to all types of vegetation and employs the following:

(1) Tree crowns are simulated as discrete geometrical objects: cone and cylinder for conifers, and spheroid for deciduous species. The non-random spatial distribution of trees is simulated using the Neyman type A distribution, which creates patchiness of a forest stand.

(2) Inside the crown, a branch architecture defined by a single inclination angle is included (Chen and Black, 1991). A branch is in turn composed of foliage elements (individual leaves in deciduous and shoots in conifer canopies) with a given angle distribution pattern.

(3) The hotspot is computed both on the ground and on the foliage with gap size distributions between and inside the crowns, respectively.

(4) The tree surface created by the crown volume (cone and cylinder, or spheroid) is treated as a complex medium

rather than a smooth surface so that shadowed foliage can be observed on the sunlit side and sunlit foliage on the shaded side.

(5) A multiple scattering scheme using view factors is used to compute the "shaded reflectivity." This scheme is essential for hyperspectral calculations because it automatically computes a spectrum of the wavelength-dependent multiple scattering factor under given canopy geometry. This makes the 5-Scale unique for hyperspectral applications.

(6) If canopy and background spectra are available, 5-Scale can output the bidirectional hyperspectral reflectance at any combination of the Sun and view geometries (Leblanc et al., 1997; 1999).

The 5-Scale model is a combination of 4-Scale by Chen and Leblanc (1997) and a leaf level spectral model. The LIBERTY model (Dawson et al., 1998) or PROSPECT (Jacquemoud et al., 1996) is currently used as the leaf-level model.

The model parameters are separated into three groups (Leblanc et al., 1999) as follows: (*i*) site parameters, including domain size, LAI, tree density, solar zenith angle, viewing angle, and relative azimuth angle; (*ii*) tree architecture parameters, including crown radius and height, apex angle, needle-to-shoot ratio, foliage clumping index, and tree foliage typical size; and (*iii*) foliage reflectance and transmittance spectra and background reflectance spectra, or band-specific reflectances and transmittance for multispectral simulations. The model calculates four surface reflectivities: sunlit and shaded foliage and sunlit and shaded backgrounds. Each reflectivity is multiplied with the viewing proportion of each component (Leblanc et al., 1999), and the total reflectivity is a sum of four components.

In several studies the 5-Scale model is demonstrated as an advanced and reliable model to be used for modelling the hotspot signature (Chen et al., 2005; Canisius and Chen, 2007). The hotspot is modelled with two kernels. One kernel uses the gap size distribution within the crowns for the canopy hotspot, and the other kernel uses the gap size distribution between the tree crowns for the background hotspot (Leblanc et al., 1999).

To improve the performance of the 5-Scale model with respect to multiangle simulations, additional functions are introduced to the model in this study. The original version of the model (before the modification) uses isotropic background reflectance values, resulting in underestimation of reflectance near the hotspot. We have incorporated the nonlinear temporal angular model (NTAM) (Latifovic et al., 2003) into 5-Scale to characterize the angular variation of the background reflectance measured in the field at one angle. This way the background reflectance becomes bidirectional, depending on the Sun–sensor geometry for each observation. The NTAM model exhibits dependence of the reflectance on satellite viewing, Sun–satellite angle, relative azimuth angle of the Sun and sensor, and solar zenith angle. The contributions of geometric and volume scattering are directly related to the amount of vegetation weighted through polynomial relationships for different land cover types. A complete description of the model can be found in Latifovic et al. (2003).

Methods

Site description and field campaign

The evaluation of the performance of the 5-Scale model is based on the CHRIS data for two different vegetation types: coniferous (black spruce) and deciduous (aspen) forests. The study area is located near Sudbury in the southern part of Ontario (47°09′47.7′′N, 81°42′23.4′′W); it is a flat area and at an elevation of approximately 350 m (**Figure 1**). During the field campaign, the black spruce sites (SB8, SB23, and SB24) were similar in appearance and considered as open canopy stands. The understory consisted of moss, Labrador tea, leatherleaf, blue bead lily, lichen, and bare soil. The aspens

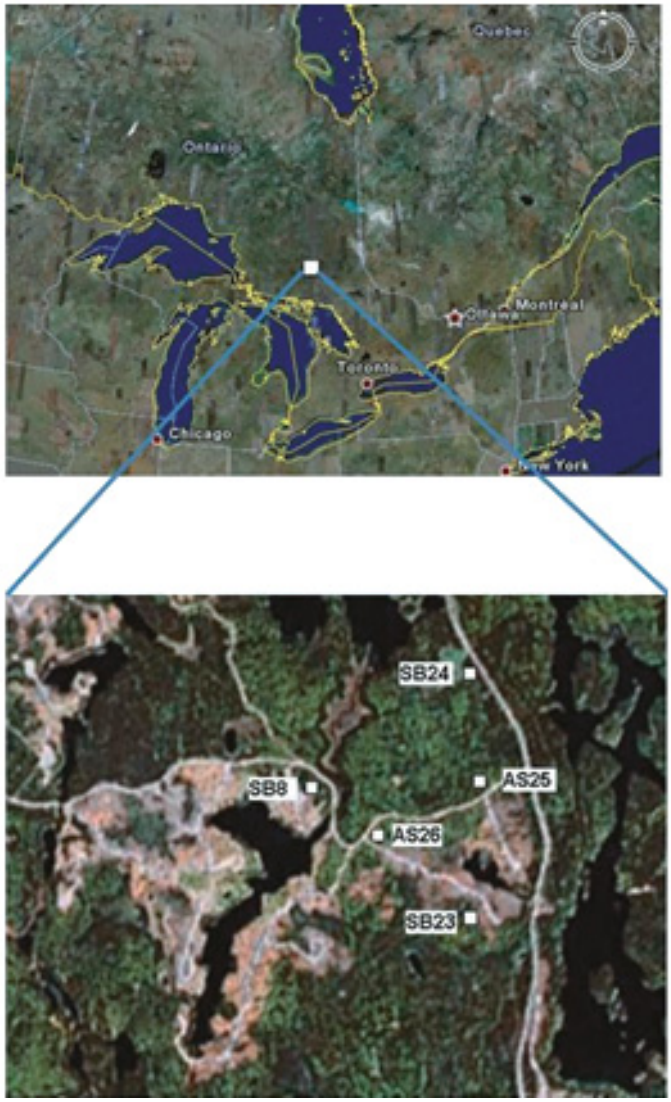

Figure 1. The study area near Sudbury, Ontario, with five study sites (three black spruce stands and two aspen stands).

sites (AS25 and AS26) were slightly different in their appearance; the trees located at AS26 were more mature with larger crowns. The understory in the aspen forests mostly contained hazelnut, maple seedlings, fern, and bare soil.

The field campaign was performed within a week of the CHRIS–PROBA overpass. The main purpose of the fieldwork was to collect various parameters to be used as inputs to 5-Scale. Over 10 sites were measured. However, due to clouds during the CHRIS–PROBA overpass, only five sites were visible in all views of the image. In each forest stand, a 30 m × 30 m plot was determined where the measurements were performed along established transects. The effective LAI data were measured using the LAI-2000 plant canopy analyzer (LI-COR, Inc., Lincoln, Nebr.) and hemispherical fish-eye photography. The LAI-2000 was operated near dusk under diffuse radiation conditions to reduce the effect of multiple scattering on the measurements. The protocol used in the measurements followed the standard instruction of the instruments (LI-COR, Inc., 1992). Clumping index was measured using tracing radiation and architecture of canopies (TRAC) (Chen and Cihlar, 1995). The ASD FieldSpectrometer (ASD, Inc., Boulder, Colo.) was used to measure the understory spectra from most common species. It was utilized in nadir measurements configuration and around solar noon, under clear sky conditions. A specially designed integrating sphere, for use with the ASD spectroradiometer, was used to measure both needle and broad leaf spectra in a field laboratory within 10 h after the leaves were collected. The integrating sphere collects reflected or transmitted light from samples over a full hemisphere where the energy is evenly spread over the entire interior surface of the sphere. A detector collects a portion of a wall energy providing the average hemispherical reflectance–transmittance. A collimated tungsten light source integrated into the sphere mimics solar irradiance. A fibre optic cable is used to connect the integrating sphere and the spectroradiometer, which measures the collected energy. The leaves were placed in Ziploc bags and refrigerated near 0 ˚C prior to the measurements of reflectance and transmittance. Structural parameters of trees (density, height, and diameter at breast height (DBH)) were also measured. The CE 318 automatic Sun tracking photometer (CIMEL Electronique) was used in the field to monitor the atmospheric aerosol concentration. The sun photometer measures Sun and sky radiance to derive aerosol properties and the total column water vapour using spectral filters; azimuth and zenith viewing angles that change during the measurements to track the Sun are controlled by a microprocessor. The sky was slightly cloudy, and extra caution was taken during the atmospheric correction of the image. The study sites were chosen to be far from the clouds to avoid the cloud edge effects.

Remote sensing data

One set of hyperspectral, multiangle CHRIS data was used in the study. The data were acquired on 10 August 2007 at 12:28 (UT) in mode 1. The dataset comprised images at five different view angles with 62 spectral bands acquired at a spatial resolution of 34 m. Solar zenith angle was 30°, and observation zenith angle was 17° (FZA = 0°), 34.25° (FZA = +36°), 39.03° (FZA = –36°), 54.51° ((FZA = +55°), and 57.51° (FZA = –55°). The solar azimuth angle was 154.4°, and the relative azimuth values were 57.67° and 51.21° for backward looking and 151.69° and 195.43° for forward looking. Minimum zenith angle was –17°. The originally received data from the ESA were radiance-at-sensor. After atmospheric corrections were applied, the surface reflectance was generated and these data were used in the analysis.

Being both hyperspectral and multiangular, CHRIS data represent a challenge to atmospheric corrections (Guanter et al., 2004; 2005a; Cutter, 2004). Calibration problems for early CHRIS data, especially around 0.50 and 0.85 µm, resulted in discrepancies at the extremes of the spectral range (Guanter et al., 2004). Despite some improvements (Guanter et al., 2007), atmospheric corrections of CHRIS data are still in the experimental phase. The 6S (Guanter et al., 2005a; Schlerf and Hill, 2005) and MODTRAN 4 (Begiebing and Bach, 2004; Guanter et al., 2007), often imbedded in software applications, are two key algorithms for atmospheric corrections of hyperspectral data. However, software applications, such as PCI and ENVI, are not always successful in correcting the atmospheric effects on CHRIS data but perform well just for specific satellite sensors for which they have built-in modules. As the first attempt in this study, ENVI Flaash was used for atmospheric corrections of CHRIS data without success. Although the resulting reflectance had reasonable values in the nadir image, the reflectance was highly negative for large view angles. Similar results were observed by Goodenough et al. (2005).

The CHRIS specific module in the Basic European Remote Sensing (ERS) and Envisat (A) along-track scanning radiometer (ATSR) and medium-resolution imaging spectrometer (MERIS) (BEAM) software (4.1 beta version, developed by Brockmann Consult, Germany) was used for making atmospheric corrections on the CHRIS data in this study. The corrections were performed by the GeoForschungsZentrum, Potsdam, Germany. Complete information about the BEAM module for CHRIS data can be found in Guanter et al. (2005a; 2005b; 2007). The important features of the module are summarized in the following.

The atmospheric correction algorithms are based on a radiative transfer approach to invert the radiance-at-sensor to the surface reflectance. As aerosol and water vapour are considered two major atmospheric constituents that impact the atmospheric scattering, algorithms for the estimation of aerosol optical thickness (AOT) and columnar water vapour (CWV) are coupled to an atmospheric radiative code. Both AOT and CWV and parameters for spectral and radiometric calibration update are derived from the data. Atmospheric oxygen and water vapour absorption features are fully resolved (Guanter, et al., 2007). Water vapour retrieval is based on a band-fitting approach where the water vapour absorption is centred at 940 nm.

Besides the atmospheric influence, the module incorporates another source of errors during the retrieval of surface reflectance such as deviation of spectral channels position and width (spectral shifts) from the nominal position. As referenced in Guanter et al. (2007), CHRIS is a pushbroom system and may cause the spectrometer entrance slit to be projected as a curve on the rectilinear detector array. Degradation in the instrument calibration can be another source of a spectral response and spectral shift. To overcome these obstacles, spectral calibration is employed in the module; the O_2 absorption feature centred at 760 nm is used as reference for this step (Guanter et al., 2007). Instrumental noise or errors in calibration (gain) coefficients (radiometric calibration) or atmospheric parameters can be an additional source of errors in the retrieved reflectance. Although applications of these algorithms in the module are dependent on the modes of CHRIS data, the complete processing suite of algorithms has been used in this study due to the fine spectral resolution of the mode 1 dataset. Therefore, the module consists of characterization of spectral calibration, AOT retrieval, CWV retrieval, reflectance retrieval, and data recalibration (Guanter et al., 2007). CHRIS data in mode 1 (and mode 5) data provide the best sampling of atmospheric absorption features in visible and NIR spectra. The adjacency effect is also considered in the correction.

In this study, the atmospheric correction module was used after the noise reduction, cloud screening, and geometric correction. A probabilistic cloud mask with the threshold of 0.05 was applied to the data. The noise removal was based on statistical analysis of the images, a method developed by Garcia and Moreno (2004). A digital elevation model (DEM) was not used because the study area is relatively flat. The aerosol optical properties were described by the rural aerosol model implemented in MODTRAN4. It was assumed that the AOT was constant over the whole scene. The water vapour images and the noise-free radiance and cloud masks images in the intermediary steps were generated. A normal rotation around the *y* axis was performed over ±36° angles during the processing.

Since no in situ multiangle measurements were available, and to ensure our confidence in the derived data, we in parallel used ATCOR 2/3 (version 6.2), developed by the German Aerospace Center and ReSe Applications, Schlapfer, Switzerland. Both BEAM and ATCOR 2/3 are based on MODTRAN-4 (Kneubuhler et al., 2005; Guanter, et al., 2007) with an imbedded atmospheric correction module for CHRIS data.

Overall approach

Based on the locations of the five study sites, corresponding reflectance values were extracted from each view angle as mean values of 3 × 3 or 2 × 2 pixel grids, depending on the size of each study plot. Measured vegetation parameters were used as the initial model parameters. Fine tuning of some parameters at the nadir view were done to bring the 5-Scale simulations as close as possible to the CHRIS nadir values. In particular, the crown radius and tree height were slightly adjusted (5%–20%), since the original values of crown radius were based on a visual approximation and the aspen trees were too high to be measured precisely. After the calibration to the nadir view data, off-nadir view simulations were performed and compared with the off-nadir CHRIS data. The backward reflectances (near the hotspot) were set to the observed zenith angles that correspond to FZA of –55° and –36°; the forward reflectances (near the darkspot) were set to the observed zenith angles that correspond to FZA of +55° and +36°. The simulations were then compared with the CHRIS data for all sites. One site for each type of forest (SB24 and AS25) was chosen to be shown in this paper.

Off-nadir hyperspectral reconstructions

To explore the redundancy in the CHRIS data, the red and NIR regions of the CHRIS data were aggregated separately within each off-nadir view based on the spectral range of the Landsat thematic mapper (TM) red and NIR bands. This is done to mimic multispectral data and validate model simulations against the CHRIS off-nadir hyperspectral measurements. Ratios in red and ratios in NIR between averages of the CHRIS measurements and 5-Scale simulations for each view angle were calculated separately. For each view, the off-nadir hyperspectral spectrum was reconstructed (denoted by $x_{\lambda,\text{new}}$) by multiplying the 5-Scale simulation with the ratios, i.e., the visible region was multiplied with the red ratio and the NIR region with the NIR ratio:

$$x_{\lambda,\text{new}} = x_{\lambda} r \tag{1}$$

where x_{λ} is the off-nadir simulation value at wavelength λ, and r is the ratio generated for the red or NIR spectrum. The red edge region was fine-tuned to match the corresponding red and NIR averages:

$$x_{\lambda,\text{new}} = x_{\lambda\text{-}2} r \tag{2}$$

These reconstructed hyperspectral values were then compared with the CHRIS measurements to demonstrate that 5-Scale can be used to reconstruct the hyperspectral spectra at off-nadir angles once it is calibrated with nadir hyperspectral and off-nadir multispectral measurements.

Method for extrapolation to the hotspot from CHRIS data

In the absence of direct satellite measurements at the hotspot, a simplified exponential model (Chen and Cihlar, 1997; Chen et al., 2005) can be used to extrapolate a measured angular point near the hotspot to the actual hotspot. This exponential hotspot model is

$$F(\xi) = C_1 \exp[-(\xi/\pi)C_2] \tag{3}$$

where $F(\xi)$ is a hotspot function, C_1 determines the magnitude of the hotspot (reflectance), and C_2 controls the width of the hotspot. C_1 is linearly related to the difference between the reflectances of the foliage and the background at the

wavelengths of interest. C_2 is proportional to the ratio of the canopy height to the size of the predominant canopy structures such as tree crowns, and the proportionality is controlled by the density of the structures such as number of stems per hectare, which is linearly related to the projected crown area index (Chen and Cihlar, 1997). The coefficients C_1 and C_2 are based on the empirical values of 1.0 and 11.0, respectively. More information about this model can be found in Chen and Cihlar (1997).

Theoretically, the exponential hotspot shape is an approximation to the reality. In many bidirectional reflectance distribution function (BRDF) models, exponential hotspot shapes are generated by assuming a mean gap size in the canopy. The 5-Scale model improves this simulation using a gap size distribution theory validated with ground measurements made by TRAC (Chen and Leblanc, 1997). Because of the inclusion of smaller and larger gaps than the mean gap, the hotspot shape simulated by 5-Scale differs from the exponential form to some small extent (Chen and Cihlar, 1997), and this difference causes errors in the extrapolation to the hotspot using the exponential function based on measurements at an angular distance from the hotspot. However, systematic studies can be conducted to minimize this error.

Using the exponential model, we assessed the error in relation to the angular distance of the measurements from the hotspot. Based on validation of 5-Scale against CHRIS data, it is reasonable to assume that the model simulates the hotspot with acceptable accuracy to be used as a basis for comparison. The assessment was based on the absolute differences between the hotspot values simulated by 5-Scale (HS_5-Scale, taken as the correct value) and by the exponential hotspot model described in Equation (3) (HS_exp). Different values of HS_exp were based on the different angular distances from the hotspot HS_5-Scale. In other words, the exponential function was fit through a number of points of the BRDF generated by 5-Scale, decreasing their distance range from 0–30° to 20–30°. The increments of the angular distance in each iteration were 1°. This increased the angular distance from zero to 20° from the hotspot, and the process resulted in 20 iterations.

Relationship between the NDHD and clumping index

Furthermore, we demonstrated that hotspot and darkspot, in addition to the nadir hyperspectral spectra, were optimal for retrieving the vegetation structural parameter, namely the clumping index. Chen et al. (2003) proposed the normalized difference between hotspot and darkspot (NDHD) as an angular index to characterize the anisotropic behaviour of foliage components as follows:

$$\mathrm{NDHD} = \frac{\rho_h - \rho_d}{\rho_h + \rho_d} \tag{4}$$

where ρ_h and ρ_d are the hotspot and darkspot reflectances, respectively.

The relationships between NDHD and the clumping index were examined in this study. An NDHD value was derived from a BRDF curve simulated by 5-Scale with a set of input parameters. In addition, we also created approximate NDHD values using near-hotspot and near-darkspot model results at distances of 5° and 10° from the corresponding hotspot and darkspot. These approximate NDHD values were also correlated with the clumping index, and then the correlations were compared to see which two angles result in the strongest relationship.

Each clumping index (Ω) was generated from the 5-Scale model using the corresponding set of input parameters (as for NDHD). The gap fraction, $P(\theta)$, at zenith angle θ, calculated in 5-Scale, was employed in the Miller (1967) theorem to calculate the effective LAI (L_e) first:

$$L_e = -2\int_0^{\pi/2} \ln[P(\theta)]\cos\theta\sin\theta\,d\theta \tag{5}$$

The clumping index was then derived using the following equation:

$$\Omega = L_e/L \tag{6}$$

where L represents LAI used as an input for a given simulation.

After the relationships were compared, we also incorporated the measured clumping index values, collected in the field, with the NDHD index based on the appropriate model input parameters. As we had only five measured clumping index values (three for black spruce stands and two for aspen stands), we did not derive a clumping index retrieval algorithm based on measurements, but rather we used the measurements to check against modelled relationships between NDHD and clumping index for conifer and deciduous forest types.

Results and discussion

Figure 2 shows the original images after destriping and atmospheric correction for sites SB24 and AS25. Due to exceptionally cloudy weather during the summer of 2007, this was the only successfully acquired dataset over the study area (**Figure 2**). Cloud shadows are not detected and corrected in this version of BEAM, and they can still be seen in the corrected data. This may cause uncertainties in the derived data, but the pixels of interest are at least 10 pixels or 340 m from the shadows except for site SB8 backward angle (–55°; not shown), for which the values from the neighbouring black spruce forest have been considered.

Atmospheric corrections are crucial, and yet challenging, for the validity of CHRIS data (Begiebing and Bach, 2004). Therefore, we also used ATCOR 2/3, additional sophisticated software for the correction of CHRIS data, to increase the confidence in the corrected results. **Figures 3** and **4** demonstrate the spectral signatures of sites SB24 (black spruce) and AS25 (aspen) after corrections using BEAM 4.1 beta version and ATCOR 2/3. The dataset corrected by BEAM 4.1 is smooth and allows meaningful calibration of 5-Scale.

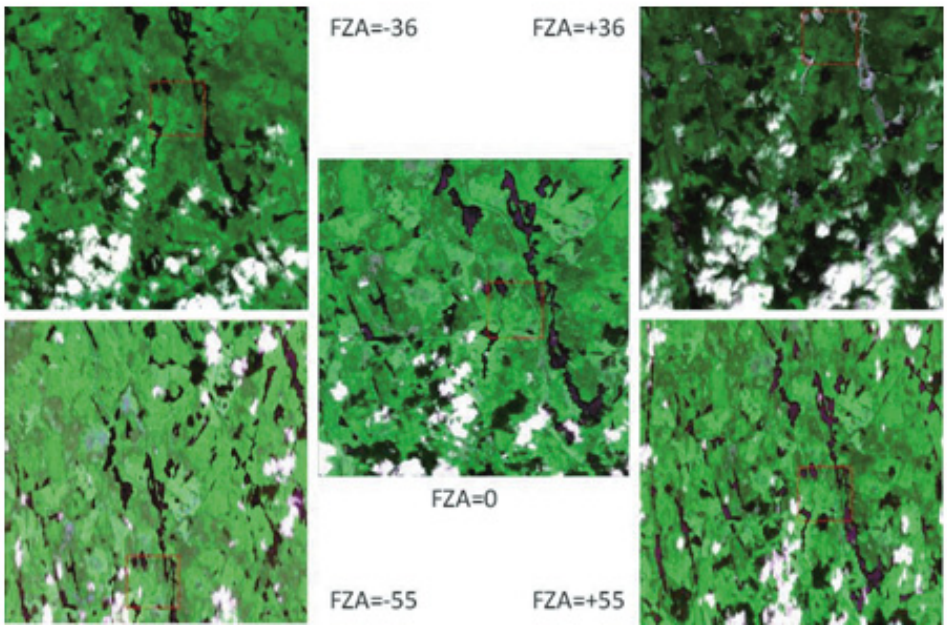

Figure 2. CHRIS data after destriping and atmospheric corrections (one nadir and four off-nadir measurements).

ATCOR 2/3 produces "spiky" curves in the NIR spectral region. However, the results suggest that there are no obvious systematic differences between the corrected signatures. Refinement of the spectral calibration within ATCOR would most likely smooth out the spikes and diminish the differences. As mentioned earlier, spectral shift occurs when the band configuration assumed in the resampling of the atmospheric parameters differs from the actual configuration. This results in errors of surface reflectance around atmospheric absorption features. The shift correction (spectral calibration) results in the smoothest surface reflectance spectrum (Guanter et al., 2007). Some uncertainties in the data are related to the assumption that the atmospheric parameters are invariant within the CHRIS image; however, this is not considered a substantial fault due to the relatively small swath (~15 km) of the sensor. Regarding the retrieval of water vapour content, the model estimation (1.8 cm) was a good fit to the ground measurements collected within 1 h of the CHRIS overpass (1.84 cm). We are not able to compare the AOT data; however, the rural atmospheric model used in the radiative transfer model is a reasonable assumption. Since no in situ multiangular measurements of surface reflectance are available, the similarity in the spectral shape and angular dependencies between the derived datasets using the two software programs give us enough confidence to use the dataset corrected by BEAM 4.1 in the proposed concept.

A good relationship between CHRIS-derived surface reflectance data using BEAM and ground reflectance measurements was found by Guanter et al. (2005b; 2007). Kneubuhler et al. (2005) also showed that CHRIS data fit well the ground measurements for meadow when ATCOR 2/3 was used for the atmospheric corrections except for some channels at 442, 905, and 1019 nm.

Generally, reflectances at the backward views (–36° and –55°) are higher than those at the nadir view in both cases, indicating the influence of the hotspot (**Figures 3**, **4**). On the other hand, reflectances at the forward views are generally lowest, as these views are near the darkspot. Different atmospheric influences on the water absorption band at 960 nm at different view angles can be seen clearly in **Figures 3** and **4**. As expected, the reflectance of the aspen stand is higher than that of the black spruce stand in NIR for all angles. A larger difference between the nadir and backward views is more pronounced within the black spruce stand than within the aspen stand. The open canopy of the black spruce stand and the exposed understory (background) enhance the hotspot reflectance. Pronounced forward scattering at FZA = +55° is shown for black spruce (**Figure 3**). This may result from very sparse vegetation and a strong influence of the soil background (Kneubuhler et al., 2005). Similar agreement between model simulations and measurements is found for all five sites (**Figures 3**, **4**). The largest disagreement (especially for sites SB8 and SB23; not shown) occurs for the FZA = +55° spectra. As summarized by Barnsley et al. (2004), scattering of optically active aerosols in the atmosphere is problematic because of a strong forward-scattering component. Typically, the least correct results from the atmospheric correction are obtained in the FZA = +55° angle, as the atmospheric influence is larger at this angle than at other angles. Furthermore, the overall reflectance levels in the data are quite low (as shown later in the paper), which enhances the errors associated with the atmospheric correction (L. Guanter, personal communication, 2007). Considering this, and the intrinsic noise and stripes associated with CHRIS, it can be concluded that the model–data agreements are quite reasonable. Because of large errors in atmospheric corrections,

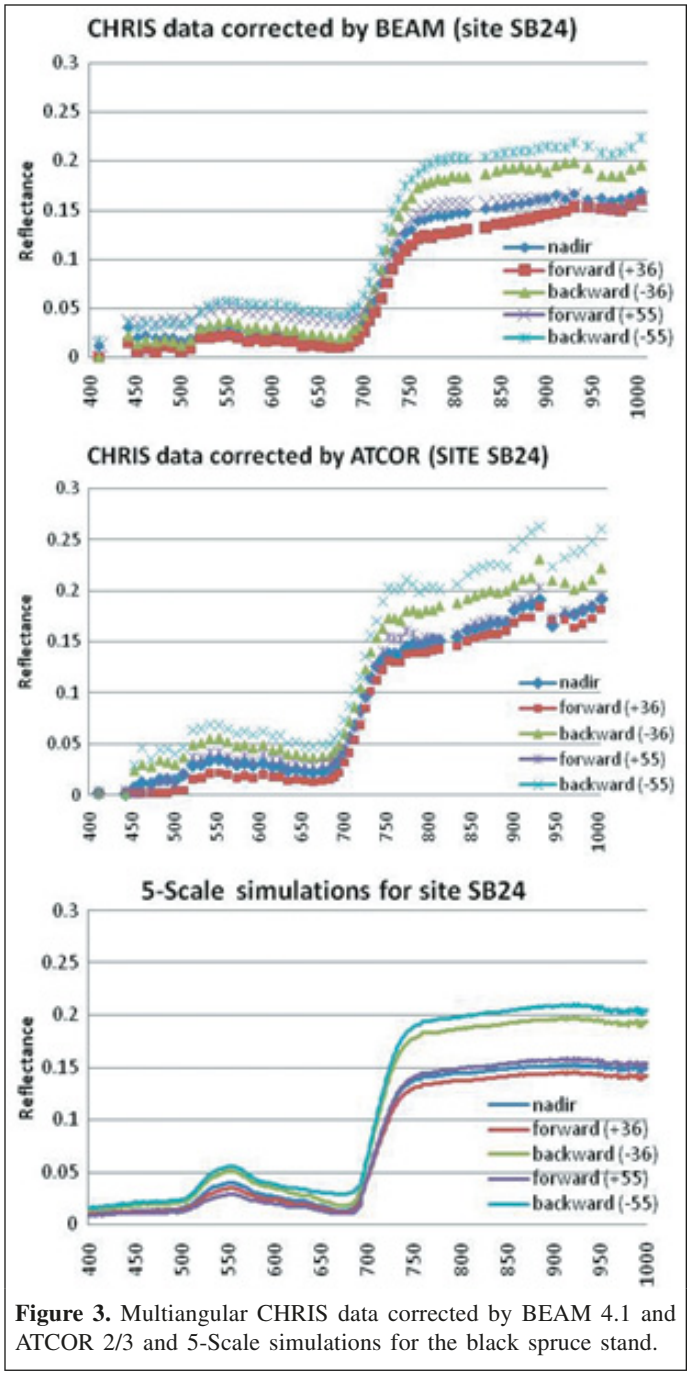

Figure 3. Multiangular CHRIS data corrected by BEAM 4.1 and ATCOR 2/3 and 5-Scale simulations for the black spruce stand.

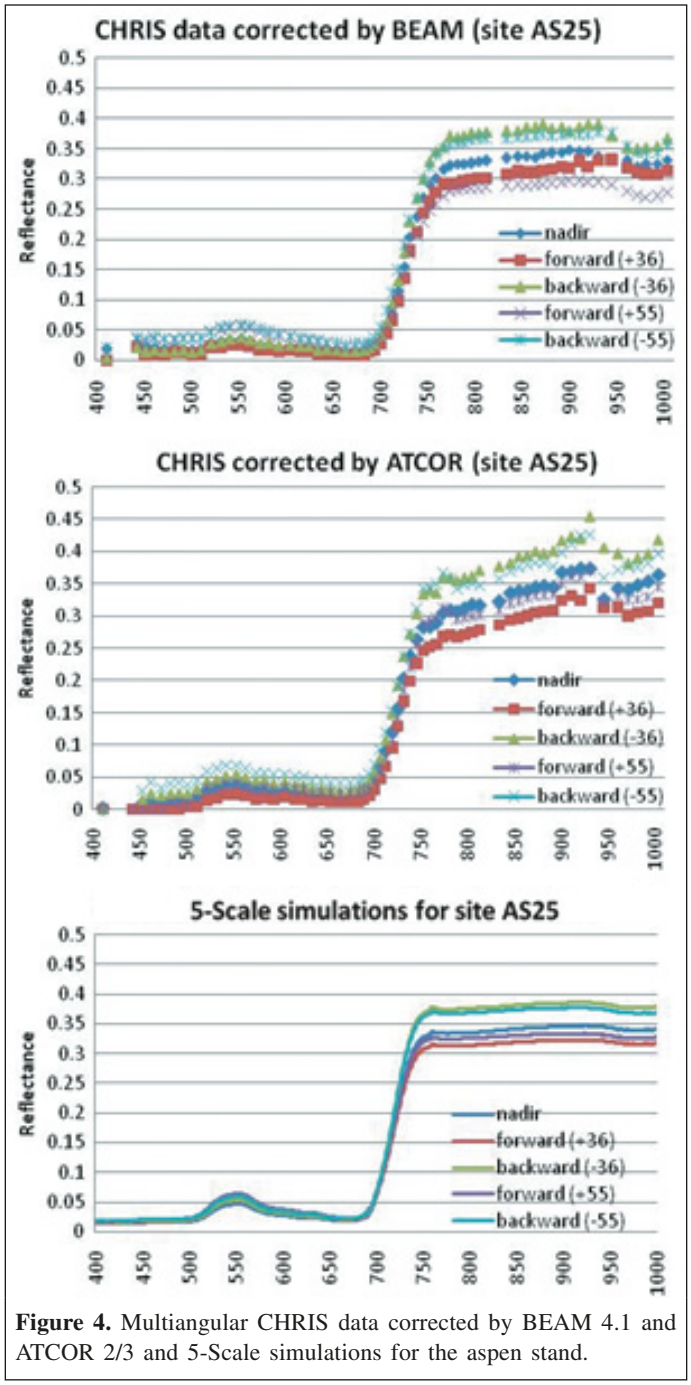

Figure 4. Multiangular CHRIS data corrected by BEAM 4.1 and ATCOR 2/3 and 5-Scale simulations for the aspen stand.

we have decided to exclude the FZA = +55° (forward) view from our analysis.

Comparison between measured CHRIS data and simulated reflectance of the canopy

Figures 5 and **6** show comparisons between modelled results and the CHRIS data for the black spruce and aspen stands for each angle. As 5-Scale has been calibrated at nadir to the CHRIS data, a close agreement, particularly for the NIR range, is shown for both stands. Some disagreement remains within the visible range and along the red edge. Most likely the disagreements at ~450, ~900, and ~1000 nm are due to the atmospheric corrections as reported by Kneubuhler et al. (2005). The reflectance at nadir for aspen is higher (~0.33) than that for black spruce (~0.15). The results for both stands are similar to those from our recent studies using compact airborne spectrographic imager (CASI) and ground data measurements. However, the reflectance is lower for all angles, particularly for black spruce, than those simulated with 5-Scale by Chen and Leblanc (2001). A reason for such low reflectance is most likely the late growing season date of the acquisition (mid-August). Although reflectance of the black spruce is not far from its peak at this time of the season (T. Noland, Ontario Ministry of Natural Resources, personal communication, 2007), due to the open canopy of this forest

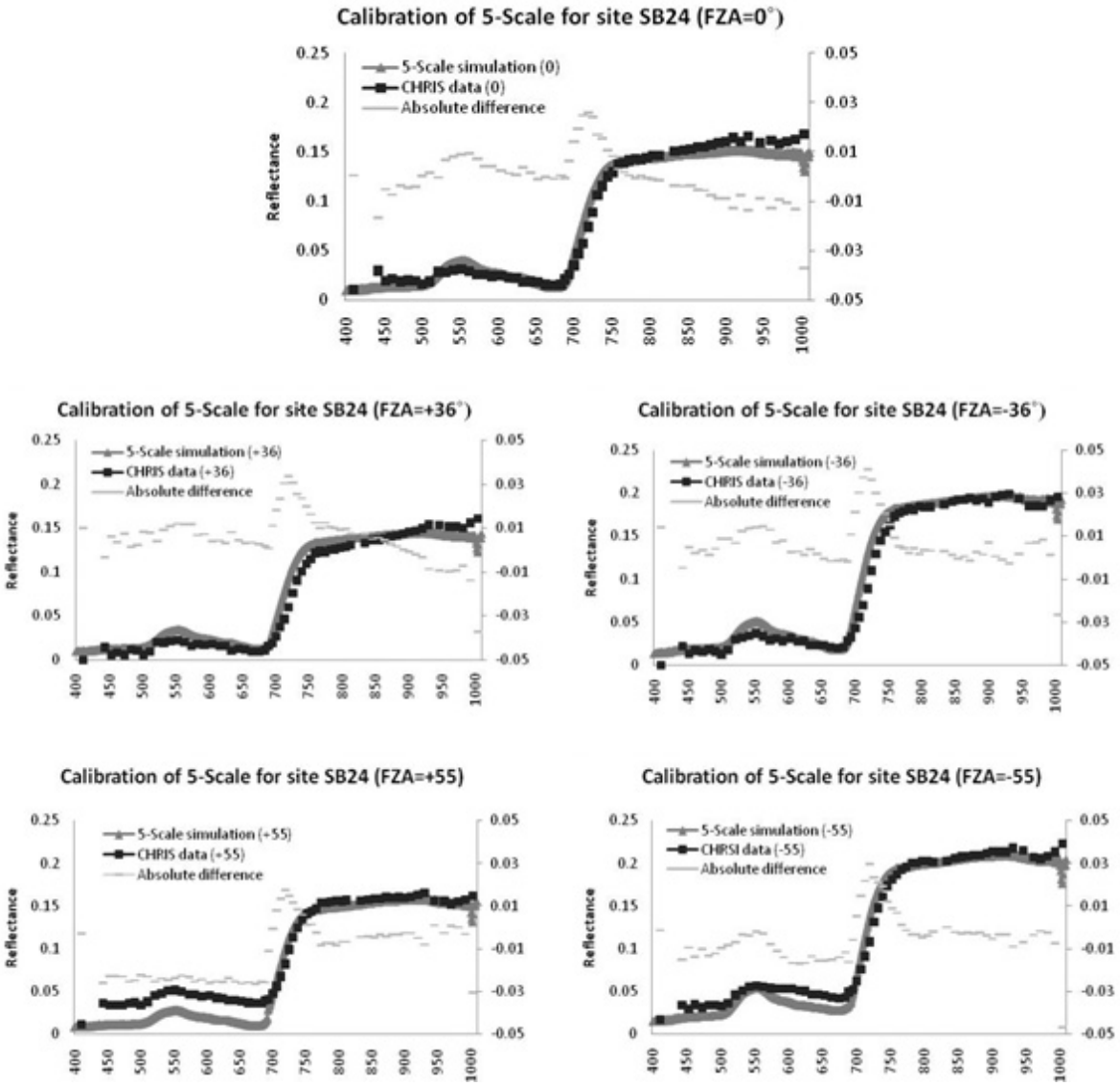

Figure 5. Agreement of the CHRIS spectra and 5-Scale simulations for black spruce at nadir and off-nadir angles. Note that the agreement between the off-nadir data was based on calibration of the nadir.

type, its understory has an effect on the overall reflectance. The understory reflectance is found to be lower during the field campaign in mid-August than the reflectance measured in late June of the same year (**Figure 7**). The seasonal differences are emphasized within the spectra of moss and leatherleaf found in the black spruce forest stands (**Figure 7**). The seasonal deterioration of the understory was also visually obvious during the field campaign. The near-hotspot spectrum (backward scattering) is closer to the nadir measurements within the aspen than within the black spruce forest, as the aspen forest is more homogeneous and has smaller gaps to expose the background (**Figure 4**). Generally, the difference between the reflectance at the nadir and FZA = –36° is larger than the difference between the reflectances at FZA = –36° and FZA = –55°, similar to the findings of Vuolo (2005).

The pattern of the simulated off-nadir spectral signatures also generally coincides with the CHRIS measurements (**Figures 5**, **6**). Most disagreement is observed between the simulated and measured signatures for the viewing angle of FZA = +55° for black spruce sites. These results confirm once again the uncertainty in the measured forward reflectance at this high view angle due to atmospheric contamination. The 5-Scale model exhibits a slight overestimation in the green spectral region and the red edge. Similar agreement of CHRIS multiangle data was determined in the first analysis of CHRIS data by Begiebing and Bach (2004), who used FourSAIL2 to simulate reflectance of maize, soil, and water. The largest disagreement in their study was observed in the red spectral region. This trend is seen mainly within the large view angles (FZA = –55°) in our study.

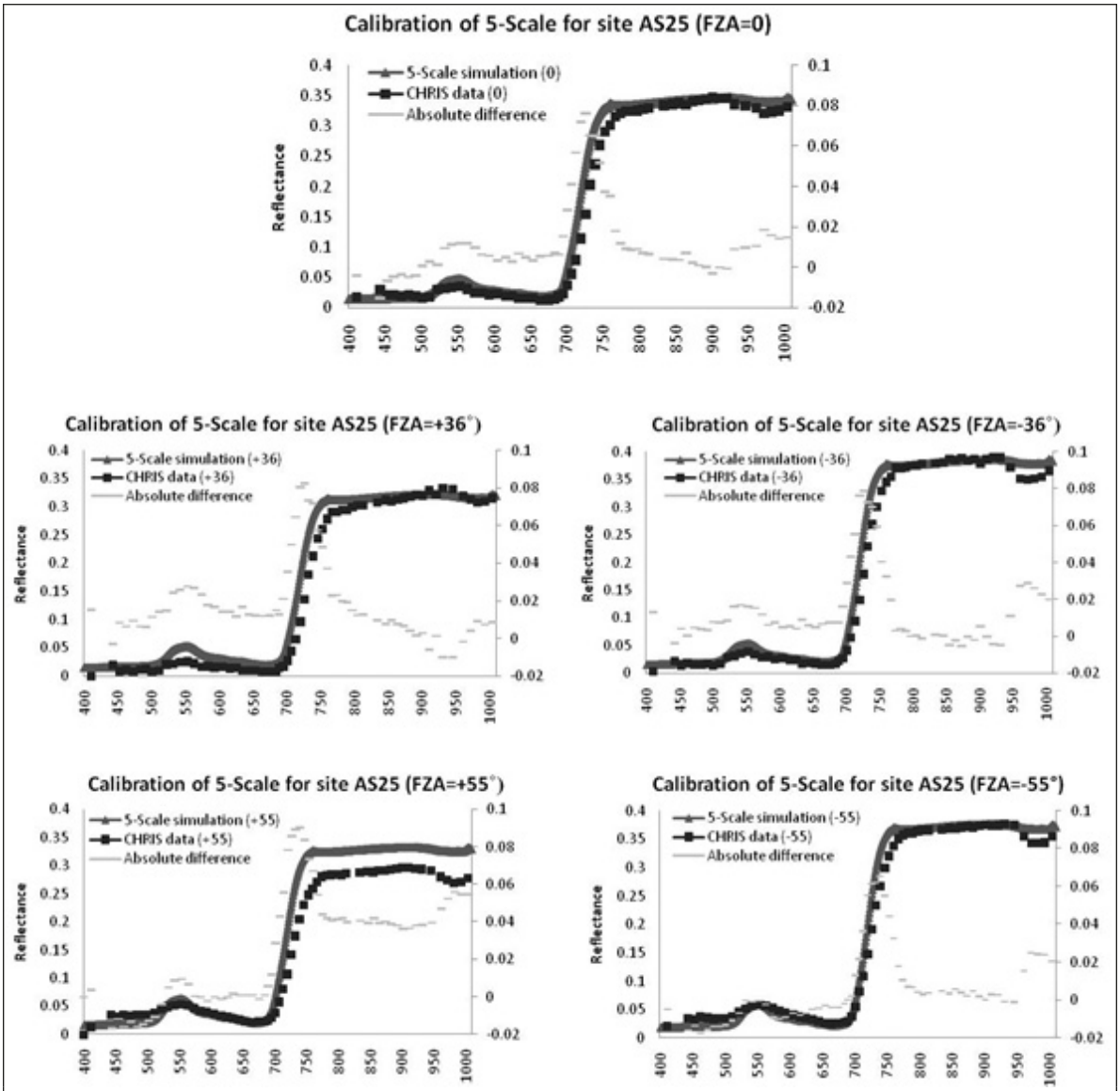

Figure 6. Agreement of the CHRIS spectra and 5-Scale simulations for aspen at the nadir and off-nadir angles. Note that the agreement between the off-nadir data was based on calibration of the nadir.

Although the true purpose of our research is not to calibrate 5-Scale using off-nadir hyperspectral data, the existing satisfactory model performance in large view angle ranges gives us further confidence that off-nadir hyperspectral signals can be simulated given the nadir hyperspectral measurements. Overall, the results show very good performance of the 5-Scale model. We feel confident in using this canopy reflectance model in our further research. For the first time in this study we have incorporated anisotropy of the background by introducing the NTAM model to 5-Scale, and this has further enhanced the performance of the model. After performing the sensitivity analysis of 5-Scale (not shown), we conclude that the model is quite sensitive to the background input spectra. D'Urso et al. (2004) also reported that understory spectra may have a considerable impact on canopy reflectance modelling and that the ability to separate understory from canopy reflectance within the CHRIS data would increase the accuracy.

Refining off-nadir 5-Scale simulations

We have conducted further research to test the proposed new measurement concept, which suggests that the CHRIS data at off-nadir views could be reconstructed from off-nadir multispectral red and NIR measurements in addition to a nadir hyperspectral spectrum (see the earlier section titled Off-nadir hyperspectral reconstructions). **Figures 8–10** demonstrate the concept. The results for the black spruce stand (**Figure 8**) illustrate that the reconstructed hyperspectral spectrum, created by adjusting the off-nadir hyperspectral simulations based on "measured" red and NIR reflectance, agree very well with the CHRIS data for all three angles. Similar results are shown for

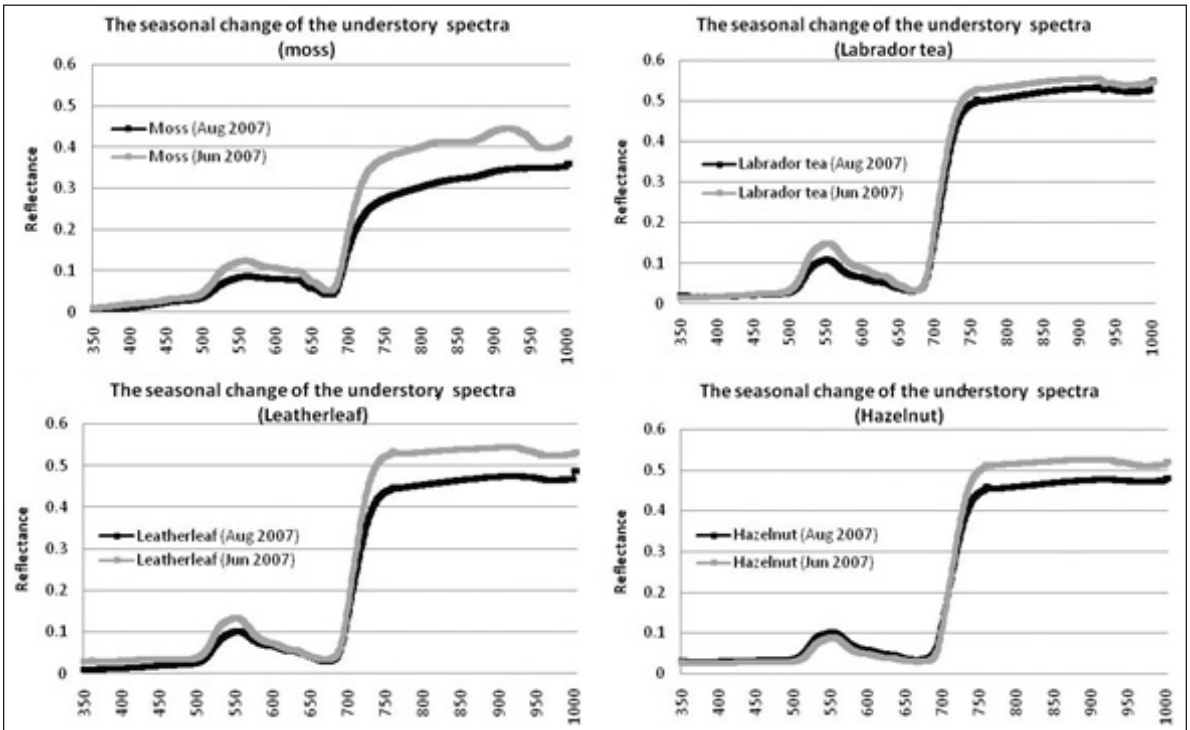

Figure 7. Seasonal changes in the understory reflectance for the most common species in the black spruce and aspen stands.

the aspen stand (**Figure 9**). These strong agreements between the reconstructed simulations and CHRIS data suggest that the CHRIS multiangle hyperspectral data exhibit redundancy. In addition, we demonstrate that measurements of off-nadir red and NIR reflectances are necessary to reduce or remove any biases in off-nadir hyperspectral simulations. **Table 1** indicates that the mean bias errors, calculated as the absolute differences, are considerably reduced when the reconstructed spectra are compared with the CHRIS spectra. Like any other models, 5-Scale cannot perfectly represent off-nadir hyperspectral reflectance. Therefore, the calibrated nadir hyperspectral reflectance and additional off-nadir multispectral reflectance are necessary and sufficient to assure accurate model performance for both nadir and off-nadir spectra. It should be noted that atmospheric correction is an important process in the evaluation of the proposed concept. For instance, the atmospherically corrected spectra for black spruce (FZA = –55°) (**Figure 8**) may introduce some uncertainties because some part of the spectra, particularly in the red region, cannot be well simulated by 5-Scale. As input background and foliage spectra to 5-Scale are reliable, the shape of the simulated canopy-level reflectance spectra should also be reliable, although the absolute values may be in error due to uncertainties in the scene component modelling. The significant departures from modelled values at localized wavelengths shown in **Figure 8** are more likely due to atmospheric influence than the model deficiency. The accuracy of atmospheric correction at red wavelengths has also influenced, to a certain extent, the reconstructed off-nadir spectra based on the aggregated red and NIR bands (see methods in the section titled Off-nadir hyperspectral reconstructions). Errors in atmospheric correction have therefore prevented us from quantifying the very weak additional information in the off-nadir hyperspectral data, if there is any. We understand from model experiments that it is highly unlikely that some spectral features in the off-nadir spectra would be missed in nadir spectra, as the nadir view is more evenly affected by all scene components than off-nadir views. This conclusion is also likely to be true for nonvegetated surfaces. However, we have only tested our concept for vegetated surfaces and for visible and NIR wavelengths, and further work is still needed to test it for longer wavelengths and for other applications of hyperspectral data, such as soil moisture assessment and mineral exploration.

According to recent research of Chen et al. (2005), two view directions useful for estimating vegetation structure are the hotspot and the darkspot. Because the real hotspot and darkspot values are not available from CHRIS images and as a summary of the previous calculations, we have used the reconstructed near-hotspot and near-darkspot spectra to elaborate the proposed concept (**Figure 10**). **Figure 10** makes it evident that the CHRIS nadir data and the reconstructed data near the hotspot and darkspot based on the simulations of 5-Scale exhibit a trend almost identical to that of the original multiangle CHRIS data (**Figures 3**, **4**).

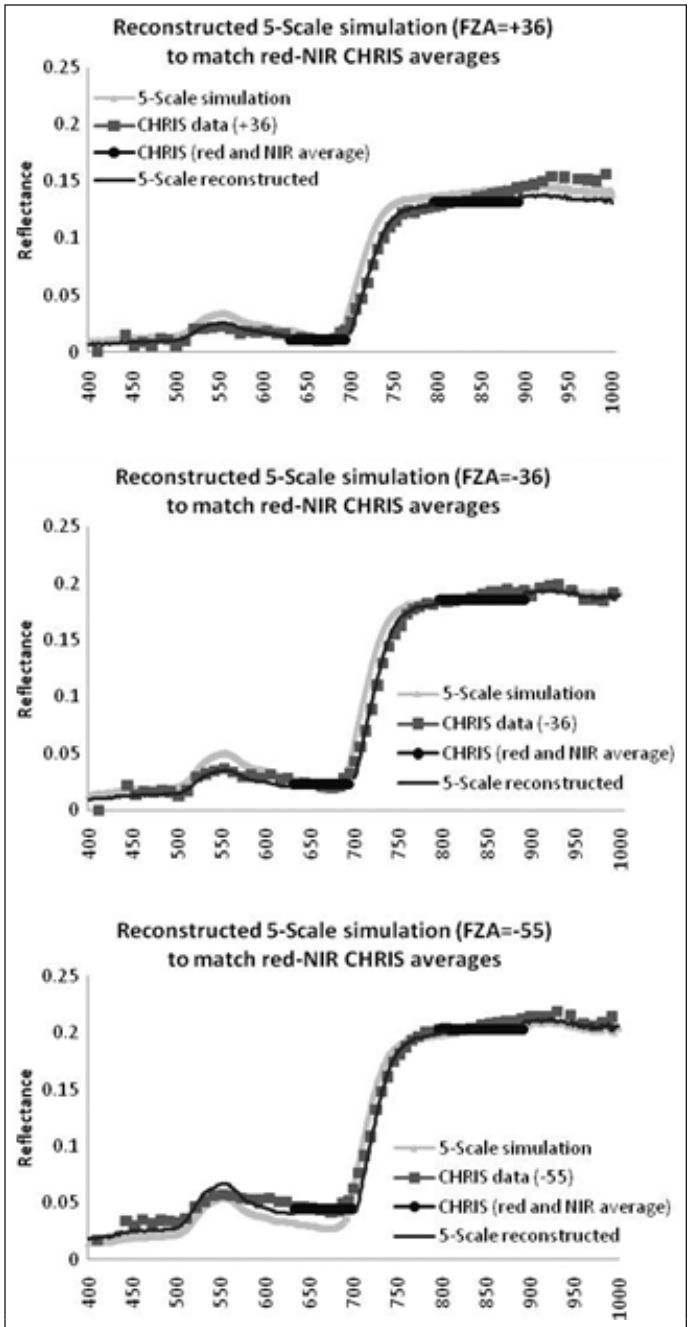

Figure 8. Reconstruction of off-nadir spectra for black spruce based on CHRIS average reflectances in aggregated red and NIR bands for FZA = +36°, –36°, and –55° using the 5-Scale model.

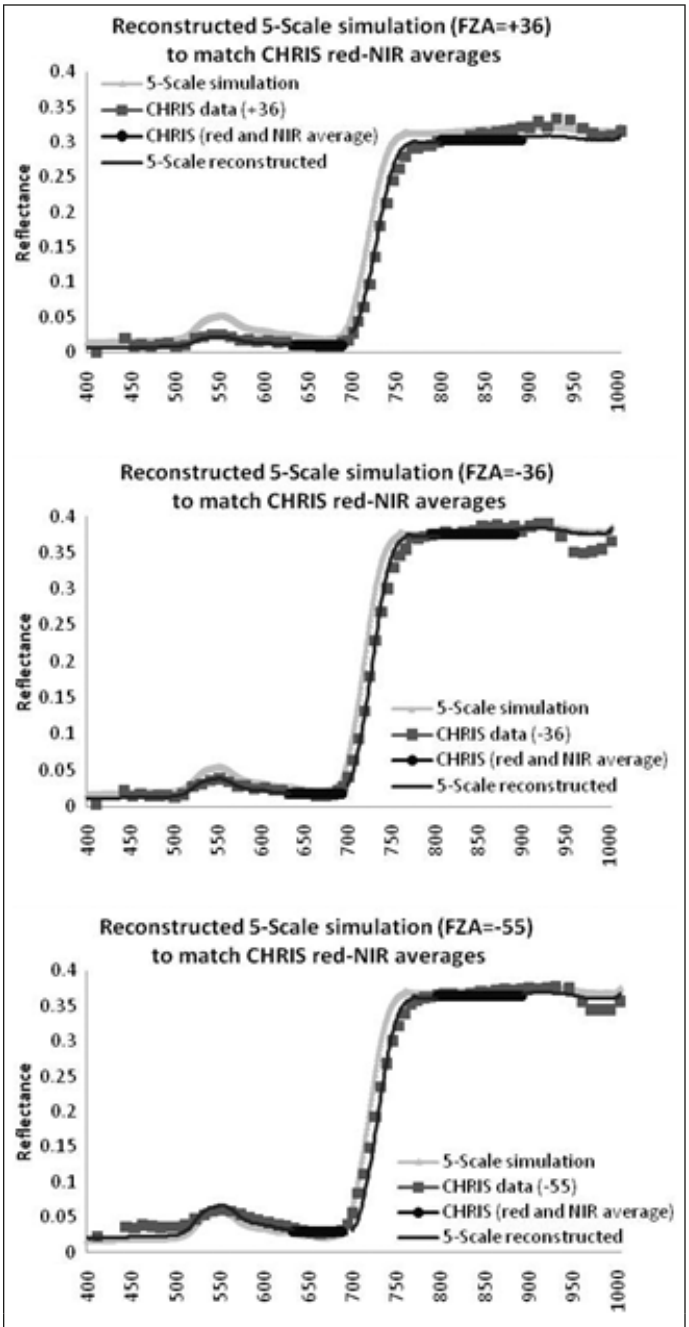

Figure 9. Reconstruction of off-nadir spectra for aspen based on CHRIS average reflectances in aggregated red and NIR bands for FZA = +36°, –36°, and –55° using the 5-Scale model.

Extrapolation to the hotspot from CHRIS measurement angles

The assessment of the error in relation to the angular distance of the measurements from the hotspot is shown in **Figure 11**, which illustrates that the error between the reflectances at the hotspot, generated by 5-Scale and approximated by the exponential function, is smallest when the angular distance is smallest (see the section titled Method for extrapolation to the hotspot from CHRIS data). If the distance from the hotspot increases (maximum of 20° in our case), the error increases. It can be noticed that the increase rate decreases with the angular distance due to the levelling of the BRDF curve farther from the hotspot. The error is minimal when the angular distance is close to the hotspot. In 5-Scale hotspot simulations, the contributions from canopy gaps smaller than the mean gap size make the hotspot sharper than the exponential form. It is found, therefore, that the hotspot determined through extrapolation using the exponential function generally underestimates the real hotspot magnitude. This underestimation increases with

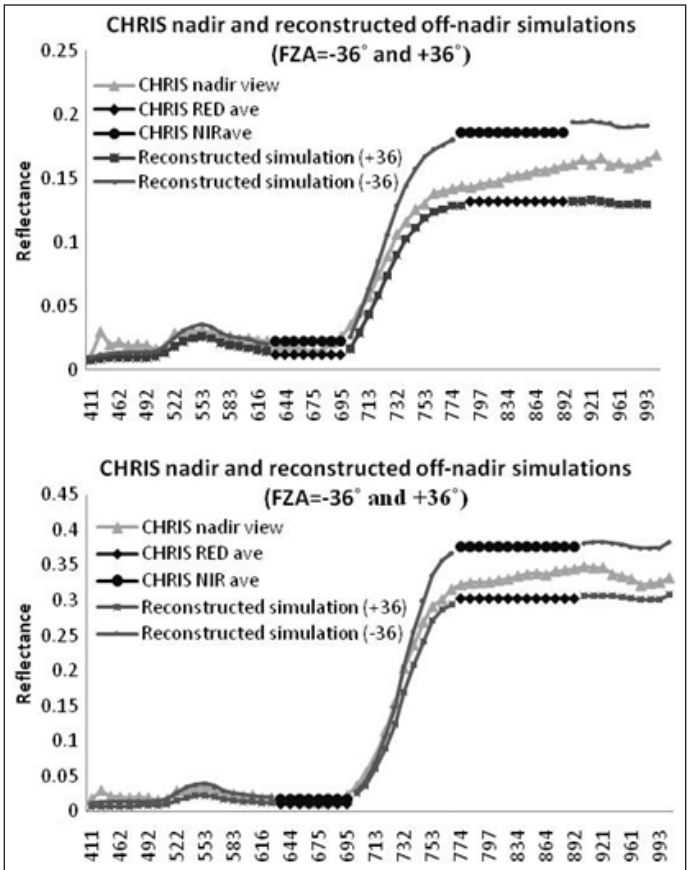

Figure 10. CHRIS nadir data and reconstructed off-nadir simulations based on CHRIS average reflectances in aggregated red and NIR bands for black spruce and aspen (nadir, +36° reconstructed, and –36° reconstructed).

Table 1. Mean bias errors (absolute difference) of the reconstructed 5-Scale simulations and the original simulations when compared with the CHRIS spectra.

		Mean bias error	
FZA (°)	Spectral region	Before reconstruction	After reconstruction
Site SB24			
36	VIS	0.006460	0.001753
	Red edge – NIR	0.019907	0.002213
–36	VIS	0.006800	–0.002390
	Red edge – NIR	0.020050	0.001640
–55	VIS	0.009700	–0.002740
	Red edge – NIR	0.011208	–0.003790
Site AS25			
36	VIS	0.014415	–0.002490
	Red edge – NIR	0.046513	0.008082
–36	VIS	0.007485	–0.001030
	Red edge – NIR	0.039007	0.001963
–55	VIS	–0.009150	–0.005030
	Red edge – NIR	0.034821	–0.006780

Note: FZA, fly-by zenith angle VIS, visible region.

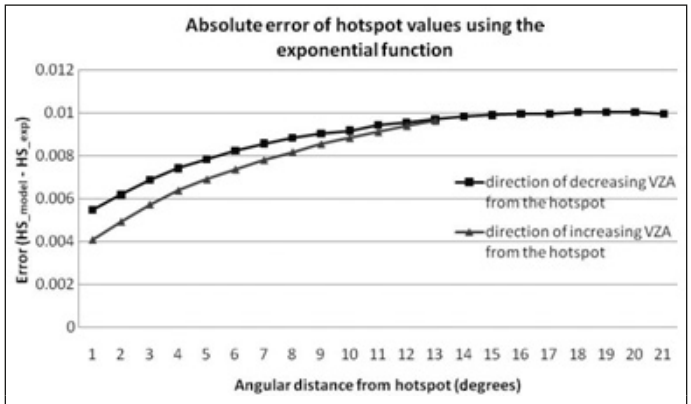

Figure 11. Absolute error of the hotspot values simulated using the exponential function in the directions of decreasing or increasing view zenith angle (VZA) from the hotspot on the principal plane.

the angular distance in both directions from the hotspot on the principal plane (**Figure 11**). This regular error pattern can therefore be used to reduce errors in hotspot determination in its application to images acquired near the hotspot.

The behaviour of the BRDF curves for black spruce simulated by 5-Scale is shown in **Figure 12a** (see the section titled Relationship between the NDHD and clumping index). The BRDFs have been generated using different values for input parameters (**Table 2**). The curves are simulated when the solar zenith angle coincides with the observing zenith angle representing a real hotspot value at 30° within the red band. The hotspot is distinct for all input parameters. The general trend suggests that the hotspot is smaller for a canopy with lower LAI and lower crown radius, even though the tree density could be high because of the increased probability of observing the ground, which has a lower reflectivity than the foliage. This trend is consistent with the finding of Chen and Leblanc (1997).

Figure 12b shows the gap fractions determined by 5-Scale using the parameters from **Table 2**. The following general pattern can be observed: the gap fraction decreases as the view zenith angle increases. We used the gap fraction to calculate the clumping index as explained in the section titled Relationship between the NDHD and clumping index. The resulting values of the clumping index are reported in **Table 2**.

To show that the hotspot and the darkspot, in addition to the nadir hyperspectral spectra, are the optimal angles for retrieving vegetation structural information, the following section explains the results of the correlation between the NDHD and the clumping index (**Figure 13**) (section titled Relationship between the NDHD and clumping index). The high correlation demonstrates the validity of 5-Scale for vegetation structural studies.

The correlation includes simulated values of the clumping index. As only three measured values of the clumping index for black spruce stands and two for aspen stands are available in this study, we don't have a sufficient number of samples to validate the simulated values. However, these five

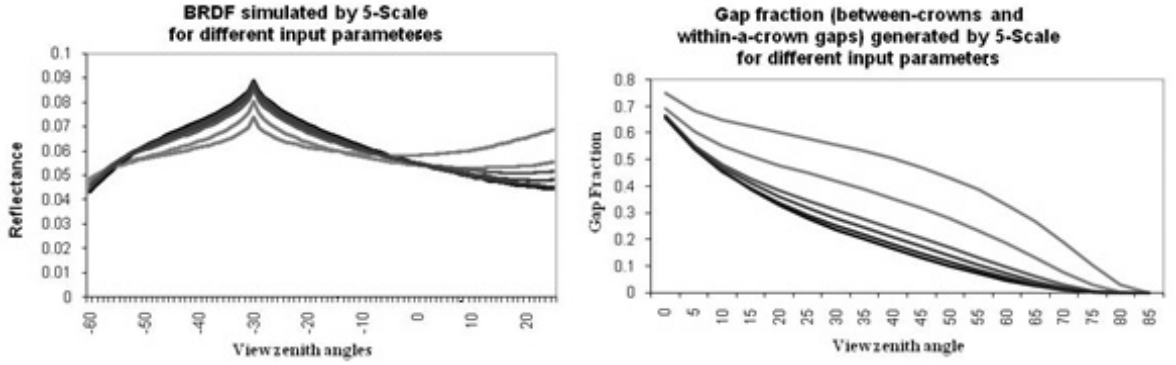

Figure 12. (a) BRDF on the principal plane simulated by the 5-Scale model for various input parameters. (b) Gap fraction simulated by the 5-Scale model for various input parameters, where LAI, tree density, and crown radius are varied. It includes between-crown and within-crown gaps.

Table 2. Ranges of the input parameters and calculated clumping index based on the Miller equation for black spruce and aspen.

Parameter	Black spruce	Aspen
LAI	1, 2, 3.3, 5, 6, 7, 8	1, 1.5, 2, 2.4, 3, 4, 5, 6
Tree density (no. of trees per hectare)	3000–6000	800–2000
Crown radius (m)	0.5–0.7	1.0–1.8
Calculated omega, Ω	0.62–0.96	0.62–0.95

measurements are added to the correlations for visual comparison, and they are compatible with modelled values. The results are in general agreement with Chen et al. (2005). The strongest correlation is between the "true" NDHD values derived from the hotspot and the darkspot (R^2 = 0.82 and 0.74 for the black spruce and aspen stands, respectively). Other approximate NDHD values, derived from near-hotspot and near-darkspot values, exhibit weaker correlations with the clumping index (**Table 3**). It can be noticed that the correlations become weaker with a greater distance from the hotspot. The distances from the darkspot have weaker impacts on the overall correlation. The correlation results for both black spruce and aspen suggest that the NDHD values based on the real hotspot and darkspot values are best for the retrieval of the clumping index (**Figure 13**). We demonstrate, through model simulations and limited validation against ground data, that the two best angles of view, in addition to nadir, are the hotspot and the darkspot, and that the multispectral measurements at these two angles would be the optimal measurement configuration for vegetation structural parameter retrieval.

This correlation may also serve as the surrogate for the validation of the hotspot and darkspot reflectance measurements. As mentioned earlier, no multiangular ground reflectance measurements are available because it very difficult to achieve this kind of ground measurement for forests. The strong relationship between NDHD, derived from the hotspot and darkspot measurements, and clumping index measured on the ground justify the validity of the multiangle measurements.

Advantages and limitations of the proposed concept

Although the concept of multiangular and hyperspectral combination has been used in the CHRIS sensor, our concept advances in several aspects: (*i*) we propose to acquire hyperspectral imagery only in the nadir direction so that the payload requirements are reduced by reducing the redundancy in the measurements because spectral signals measured at different angles are highly correlated, as demonstrated by the CHRIS measurements; and (*ii*) we propose to acquire two-band images (red and NIR would be sufficient) in two specific directions of importance in retrieving vegetation structure, namely the hotspot and darkspot, based on our recent research results. This proposed concept is a refinement of the existing sensor. However, it requires technical development to synchronize the hotspot and darkspot multispectral measurements with the local solar zenith angle along the satellite orbit, and to measure the hotspot for a large latitudinal range within one orbit, the conventional morning local overpass time for Sun-synchronous polar orbits may need to be changed (see explanation to follow). The investment in meeting these technical requirements may be evaluated against the information gain from this new measurement concept.

We realized that in an actual orbit it is impossible to measure the hotspot and nadir for the same swath within the same overpass unless the local overpass time is noon. We therefore need to modify the orbit to have near noon overpass time at the equator in a Sun-synchronous orbit. We propose to have two additional multispectral (red and NIR) cameras. One is forward looking at 20°–60° to the zenith on the ground to acquire the darkspot, and the other is backward looking at the local solar zenith angle. As the darkspot can be measured in a large range from 20° to 60° zenith angle, it should also be synchronized with the solar position to be at the opposite side of the Sun on the principal solar plane. The hotspot direction changes with the local solar zenith angle, and thus the backward-looking camera view zenith angle has to progressively decrease as the satellite moves south along the orbit. Additional attention should be given to the directions of the cameras when overpassing the southern hemisphere to synchronize hotspot

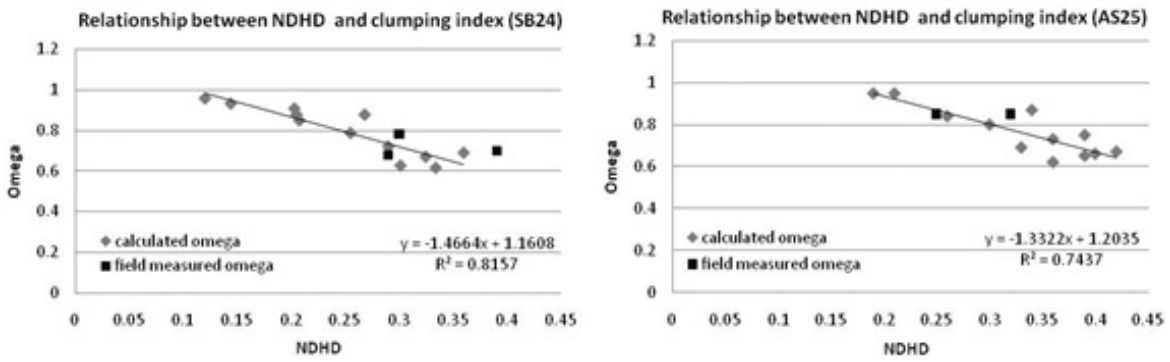

Figure 13. Relationships between NDHD and clumping index for the black spruce and aspen stands.

Table 3. Relationships between NDHD and clumping index for black spruce and aspen when approximate reflectance values near the hotspot and darkspot (at various angular distances) are used to construct NDHD without extrapolating to the hotspot and darkspot.

	R^2	
Approximate NDHD index	Black spruce	Aspen
5° from the hotspot and darkspot	0.77	0.71
10° from the hotspot and darkspot	0.69	0.60
5° and 10° from the hotspots and darkspots	0.76	0.67

and darkspot directions because both cameras have to move across the zenith on the principal solar plane (or within ±15° from the solar plane). One limitation of the system is that when the Sun is at the zenith, the hotspot camera will view in the nadir direction and overlap with the nadir hyperspectral sensor. The system would work the best when the solar zenith angle is larger than 20°.

Conclusions

The main goal of this study was to investigate the feasibility of an emerging technology that employs the combination of multiangle and hyperspectral remote sensing. We proposed to add two additional angles of measurements in two spectral bands to a nadir hyperspectral imager. This study attempted to develop a new Earth observation concept of combining nadir hyperspectral remote sensing with hotspot and darkspot multispectral measurements to characterize simultaneously the structure and biochemical properties of vegetation. This system would be a refinement of an existing multiangle hyperspectral sensor, namely the compact high-resolution imaging spectrometer (CHRIS). The refinement was proposed to reduce the redundancy of hyperspectral data at more than one angle and to better retrieve the three-dimensional vegetation structural information by choosing the two most useful angles of measurements.

The 5-Scale model was successfully used to simulate multiangle spaceborne remote sensing data. Very good agreements between CHRIS hyperspectral data and modelled canopy reflectance spectra were shown for nadir and most off-nadir angles. Furthermore, we successfully demonstrated that off-nadir spectral simulations could be brought to very close agreement with the CHRIS data once multispectral measurements at off-nadir angles were available for further model calibration. The remaining model errors were considerably smaller than errors introduced by atmospheric correction using state-of-the-art software. This demonstrated that off-nadir hyperspectral data were mostly redundant for vegetation applications and that multispectral measurements at off-nadir angles (hotspot and darkspot, in particular), in addition to nadir hyperspectral data, provided optimal vegetation structure retrieval accuracy.

Based on 5-Scale simulations, we also demonstrated that hotspot and darkspot were the two best angles to measure from space for foliage clumping index estimation. The 5-Scale model was shown to be capable of qualitatively representing off-nadir reflectance spectra. Based on the findings in this and previous research, we believe that two-band measurements near the hotspot and darkspot are the best options for further calculations and estimations of the clumping index. This vegetation structural parameter would be essential for retrieving other vegetation information including the leaf chlorophyll content.

A simple exponential function was tested for extrapolating measurements made near the hotspot to the hotspot. An error pattern as a function of the angular distance from the hotspot was observed. This permits reliable estimation of the hotspot value for every pixel of a scene acquired at a small angular distance from the hotspot, proving that our methodology of deriving structural parameters using the hotspot and darkspot measurements is practically feasible, even though in practice measurements may not be made exactly at the hotspot, and the angular distance from the hotspot may vary between pixels.

This study serves to initiate the evaluation of our proposed new measurement concept. In our evaluation using CHRIS data over forests, the atmospheric influence has not been completely removed, casting some uncertainties in model ability to reconstruct hyperspectral data at large zenith angles. Further research in atmospheric correction and in evaluating the concept using airborne imagery would be useful in this context.

If this concept is adopted, the satellite orbit needs to be scheduled in such a way that the local overpass time is near the solar noon so that measurements can be made as near to the hotspot as possible. Both cameras for the hotspot and the darkspot need to be synchronized with the Sun so that one is observing near the hotspot and the other is observing the darkspot. One limitation of the system is that when the Sun is at the zenith, the hotspot camera will view in the nadir direction and overlap with the nadir hyperspectral sensor. The system would work best when the solar zenith angle is larger than 20°. This system could potentially be used as an additional feature to the proposed hyperspectral environmental and resource observer (HERO) mission or may be considered by other land observation missions acquiring vegetation structural information. Combining hyperspectral with multiangle data would provide the opportunity for simultaneous retrieval of vegetation structural and biochemical parameters, improving the accuracy of hyperspectral applications.

Acknowledgements

We thank Dr. Dave Goodenough, Dr. Martin Bergeron, and Mr. Andrew Dyk for useful inputs during the process of atmospheric corrections of the CHRIS data. We also thank Dr. Jose Moreno from University of Valencia and Dr. Luis Guanter and Luis Gomez for processing the data with the BEAM software. Peter Fletcher put some great effort in coordinating the CHRIS acquisitions, and Dr. Tom Noland, Jan Pisek, and Emil Zelic were of great help in accomplishing the fieldwork. Dr. John Miller and Jim Freemantle provided us with some field instruments and in-depth instruction on their use. We thank the European Space Agency (ESA) for the CHRIS data and the Canadian Space Agency (CSA) for funding to conduct this research.

References

Bach, H., Begiebing, S., Waldmann, D., and Rowotzki, B. 2005. Analyses of hyperspectral and directional data for agricultural monitoring using a canopy reflectance model SLC; progress in the Upper Rhine valley and Baasdorf test-sites. In *Proceedings of the 3rd CHRIS/Proba Workshop*, 21–23 March 2005, ESRIN, Frascati, Italy. Edited by H. Lacoste. ESA SP-593, ESA Publications, ESTEC, Noordwijk, The Netherlands.

Bajwa, S.G., Bajcsy, P., Groves, P., and Tian, L.F. 2004. Hyperspectral image data mining for bands selection in agricultural applications. *Transactions of the ASAE*, Vol. 47, No. 3, pp. 895–907.

Barnsley, M.J., Settle, J.J., Cutter, M.A., Lobb, D.R., and Teston, F. 2004. The PROBA/CHRIS Mission: A low-cost smallsat for hyperspectral multiangle observations of the earth surface and atmosphere. *IEEE Transactions on Geoscience and Remote Sensing*, Vol. 42, No. 7, pp. 1512–1520.

Begiebing, S., and Bach, H. 2004. Analyses of hyperspectral and directional CHRIS data for agricultural monitoring using a canopy reflectance model. In *Proceedings of the 2nd CHRIS/Proba Workshop*, 28–30 April 2004, ESRIN, Frascati, Italy. Compiled by H. Lacoste. ESA SP-578, ESA Publications, ESTEC, Noordwijk, The Neatherlands.

Begiebing, S., Bach, H., Waldmann, D., and Mauser, W. 2005. Analyses of spaceborne hyperspectral and directional CHRIS data to deliver crop status for precision agriculture. In *Proceedings of the 5th European Conference on Precision Agriculture*, 9–12 June 2005, Uppsala, Sweden. Edited by J. Stafford and A. Werner. Wageningen Academic Publishers, Wageningen, The Netherlands. pp. 227–234.

Canisius, F., and Chen, J. 2007. Retrieving forest background reflectance in a boreal region from multi-angle imaging spectroradiometer (MISR) data. *Remote Sensing of Environment*, Vol. 107, pp. 312–321.

Chen, J.M., and Black, T.A. 1991. Measuring leaf area index of plant canopies with branch architecture. *Agricultural and Forest Meteorology*, Vol. 57, pp. 1–12.

Chen, J., and Cihlar, J. 1995. Plant canopy gap size analysis theory for improving optical measurements of leaf area index. *Applied Optics*, Vol. 34, pp. 6211–6222.

Chen, J.M., and Cihlar, J. 1997. A hotspot function is a simple bidirectional reflectance model for satellite applications. *Journal of Geophysical Research*, Vol. 102, pp. 25 907 – 25 913.

Chen, J.M., and Leblanc, S.G. 1997. A four-scale bidirectional reflectance model based on canopy architecture. *IEEE Transactions on Geoscience and Remote Sensing*, Vol. 35, pp. 1316–1337.

Chen, J.M., and Leblanc, S.G. 2001. Multiple-scattering scheme useful for geometric optical modeling. *IEEE Transactions on Geoscience and Remote Sensing*, Vol. 39, No. 5, pp. 1061–1071.

Chen, J.M., Liu, J., Leblanc, S.G., Lacaze, R., and Roujean, J.-L. 2003. Multi-angular optical remote sensing for assessing vegetation structure and carbon absorption. *Remote Sensing of Environment*, Vol. 84, pp. 516–525.

Chen, J.M., Menges, C.H., and Leblanc, S.G. 2005. Global mapping of foliage clumping index using multi-angular satellite data. *Remote Sensing of Environment*, Vol. 97, pp. 447–457.

Cierniewski, J., Gdala, T., and Karnieli, A. 2004. A hemispherical–directional reflectance model as a tool for understanding image distinctions between cultivated and uncultivated bare surfaces. *Remote Sensing of Environment*, Vol. 90, pp. 505–523.

Costa, S., and Fiori, S. 2001. Image compression using principal component neural networks. *Image and Vision Computing*, Vol. 19, No. 9–10, pp. 649–668.

Cutter, M. 2004. Review of aspects associated with the CHRIS calibration. In *Proceedings of the 2nd CHRIS/Proba Workshop*, 28–30 April 2004, ESRIN, Frascati, Italy. Compiled by H. Lacoste. ESA SP-578, ESA Publications, ESTEC, Noordwijk, The Netherlands.

Dawson, T.P., Curran, J.P., and Plummer, S.E. 1998. LIBERTY — Modeling the effects of leaf biochemical concentration on reflectance spectra. *Remote Sensing of Environment*, Vol. 65, No. 1, pp. 50–60.

Deering, D.W., Eck, T.F., and Banerjee, B. 1999. Characterization of the reflectance anisotropy of three boreal forest canopies in spring–summer. *Remote Sensing of Environment*, Vol. 67, pp. 205–229.

D'Urso, G., Dini, L., Vuolo, F., Alonso, L., and Guanter, L. 2004. Retrieval of leaf area index by inverting hyperspectral multi-angular CHRIS/Proba data from SPARC 2003. In *Proceedings of the 2nd CHRIS/Proba Workshop*, 28–30 April 2004, ESRIN, Frascati, Italy. Compiled by H. Lacoste. ESA SP-578, ESA Publications, ESTEC, Noordwijk, The Netherlands.

Dyk, A., Goodenough, D.G., Li, J.Y., Niemann, K.O., Guan, A., Chen, H., and Duong, J. 2005. Multi-temporal, multi-angle evaluation with CHRIS of coastal forests. In *IGARSS'05, Proceedings of the International Geoscience*

and Remote Sensing Symposium, 24–29 July 2005, Seoul, Korea. IEEE, Piscataway, N.J.

Gao, F., Schaaf, C.B., Strahler, A.H., Jin, Y., and Li, X. 2003. Detecting vegetation structure using a kernel-based BRDF model. *Remote Sensing of Environment*, Vol. 86, pp. 198–205.

Garcia, J.C., and Moreno, J. 2004. Removal of noises in CHRIS/Proba images: Application to the SPARC campaign data. In *Proceedings of the 2nd CHRIS/Proba Workshop*, 28–30 April 2004, ESRIN, Frascati, Italy. Compiled by H. Lacoste. ESA SP-578, ESA Publications, ESTEC, Noordwijk, The Netherlands.

Goodenough, D.G., Dyk, A., Han, T., Chen, H., Gates, T., and Niemann, K.O. 2005. Multi-temporal evaluation with CHRIS of coastal forests. In *IGARSS'05, Proceedings of the International Geoscience and Remote Sensing Symposium*, 24–29 July 2005, Seoul, Korea. IEEE, Piscataway, N.J.

Guanter, L., Alonso, L., and Moreno, J. 2004. Atmospheric corrections of CHRIS/Proba data acquired in the SPARC Campaign. In *Proceedings of the 2nd CHRIS/Proba Workshop*, 28–30 April 2004, ESRIN, Frascati, Italy. Compiled by H. Lacoste. ESA SP-578, ESA Publications, ESTEC, Noordwijk, The Netherlands.

Guanter, L., Alonso, L., and Moreno, J. 2005a. A method for the surface reflectance retrieval from PROBA/CHRIS data over land: Application to ESA SPARC campaigns. *IEEE Transactions on Geoscience and Remote Sensing*, Vol. 43, No. 12, pp. 2908–2917.

Guanter, L., Alonso, L., and Moreno, J. 2005b. First results from the PROBA/CHRIS hyperspectral/multiangular satellite system over land and water targets. *IEEE Geoscience and Remote Sensing Letters*, Vol. 2, No. 3, pp. 250–254.

Guanter, L., Alonso, L., Gomez-Chova, L., and Moreno, J. 2007. CHRIS/PROBA atmospheric correction module. Algorithm Theoretical Basis Document, ESA ITT SoWENVI-DTEX-EOPS-SW-06-0008, ESA Publications, ESTEC, Noordwijk, The Netherlands.

Guo, B., Gunn, S., Damper, B., and Nelson, J. 2005. Hyperspectral image fusion using spectrally weighted kernels. In *Proceedings of the 7th International Conference on Information Fusion*, June 2004, Stockholm, Sweden. Edited by P. Svensson and J. Schubert. IEEE, Piscataway, N.J.

Jacquemoud, S., Ustin, S.L., Verdebout, J., Scmuck, G., Andreoli, G., and Hosgood, B. 1996. Estimating leaf biochemistry using the PROSPECT leaf optical properties model. *Remote Sensing of Environment*, Vol. 56, pp. 194–202.

Kneubuhler, M., Koetz, B., Richter, R., Schaepmann, M., and Itten, K. 2005. Geometric and radiometric pre-processing of CHRIS/Proba data over mountainous terrain. In *Proceedings of the 3rd CHRIS/Proba Workshop*, 21–23 March 2005, ESRIN, Frascati, Italy. Edited by H. Lacoste. ESA SP-593, ESA Publications, ESTEC, Noordwijk, The Netherlands.

Kumar, R., and Makkapati, V. 2005. Encoding of multispectral and hyperspectral image data using wavelet transform and gain shape vector quantization. *Image and Vision Computing*, Vol. 23, pp. 721–729.

Latifovic, R., Cihlar, J., and Chen, J.M. 2003. A comparison of BRDF models for the normalization of satellite optical data to a standard Sun–target–sensor geometry. *IEEE Transactions on Geoscience and Remote Sensing*, Vol. 41, No. 8, pp. 1889–1898.

Leblanc, S.G., Chen, J.M., and Cihlar, J. 1997. Directionality of NDVI in boreal forests. *Canadian Journal of Remote Sensing*, Vol. 23, pp. 369–380.

Leblanc, S.G., Bicheron, P., Chen, J.M., Leroy M., and Cihlar, J. 1999. Investigation of directional reflectance in boreal forests using an improved 4-Scale model and airborne POLDER data. *IEEE Transactions on Geoscience and Remote Sensing*, Vol. 37, No. 3, pp. 1396–1414.

Lewis, P., Barnsley, M.J., and Cutter, M. 2001. CHRIS/PROBA: Mission status and prospects for mapping surface biophysical parameters. In *IGARSS'01, Proceedings of the International Geoscience and Remote Sensing Symposium*, 9–13 July 2001, Sydney, Australia. Edited by T.I. Stein. IEEE, Piscataway, N.J.

LI-COR, Inc. 1992. *LAI-2000 plant canopy analyzer operating manual*. LI-COR, Inc., Lincoln, Nebr.

Miller, J.B. 1967. A formula for average foliage density. *Australian Journal of Botany*, Vol. 15, pp. 141–144.

Motta, G., Rizzo, F., and Storer, J.A. 2006. *Hyperspectral data compression*. Springer, New York.

Rautiainen, M., Stenberg, P., Nilson, T., and Kuusk, A. 2004. The effect of crown shape on the reflectance of coniferous stands. *Remote Sensing of Environment*, Vol. 89, pp. 41–52.

Sandmeier, S., and Deering, D.W. 1999. Structure analysis and classification of boreal forests using airborne hyperspectral BRDF data from ASAS. *Remote Sensing of Environment*, Vol. 69, pp. 281–295.

Schlerf, M., and Hill, J. 2005. Estimation of forest biophysical characteristics through coupled atmosphere–reflectance model inversion using hyperspectral multi-directional remote sensing data — A contribution to future forest inventory strategies. In *Proceedings of the 3rd CHRIS/Proba Workshop*, 21–23 March 2005, ESRIN, Frascati, Italy. Edited by H. Lacoste. ESA SP-593, ESA Publications, ESTEC, Noordwijk, The Netherlands.

Smith, M.L., Martin, M.E., Plourde, L, and Ollinger, S.V. 2003. Analysis of hyperspectral data for estimation of temperate forest canopy nitrogen concentration: comparison between an airborne (AVIRIS) and a spaceborne (Hyperion) sensor. *IEEE Transactions on Geoscience and Remote Sensing*, Vol. 41, No. 6, pp. 1332–1337.

Townsend, P.A., Foster, J.R., Chastain, R.A., Jr., and Currie, W.S. 2003. Application of imaging spectroscopy to mapping canopy nitrogen in the forest of the central Appalachian Mountains using Hyperion and AVIRIS. *IEEE Transactions on Geoscience and Remote Sensing*, Vol. 41, No. 6, pp. 1347–1353.

Treitz, P.M., and Howarth, P.J. 1999. Hyperspectral remote sensing for estimating biophysical parameters of forest ecosystems. *Progress in Physical Geography*, Vol. 23, No. 3, pp. 359–390.

Vuolo, F., Dini, L., and D'Urso, G. 2005. Assessment of LAI retrieval accuracy by inverting art model and a simple empirical model with multiangular and hyperspectral CHRIS/Proba data from SPARC. In *Proceedings of the 3rd CHRIS/Proba Workshop*, 21–23 March 2005, ESRIN, Frascati, Italy. Edited by H. Lacoste. ESA SP-593, ESA Publications, ESTEC, Noordwijk, The Netherlands.

Widlowski, J-L., Pinty, B., Gobron, N., Verstraete, M.M., Diner, D.J., and Davis, A.B. 2004. Canopy structure parameters derived from multi-angular remote sensing data for terrestrial carbon studies. *Climatic Change*, Vol. 67, pp. 403–415.

Zhang, Y., Tian, Y., Myneni, R.B., Knyazikhin, Y., and Woodcock, C.E. 2002. Assessing the information content of multiangle satellite data for mapping biomes: I. Statistical analysis. *Remote Sensing of Environment*, Vol. 80, pp. 418–434.